Mechanical Systems and Signal Processing (2001) **15**(2), 337–356
doi:10.1006/mssp.2000.1346, available online at http://www.idealibrary.com on IDEAL®

WAVELET ANALYSIS TO CHARACTERISE NON-LINEARITIES AND PREDICT LIMIT CYCLES OF AN AEROELASTIC SYSTEM

RICK LIND, KYLE SNYDER AND MARTY BRENNER
NASA Dryden Flight Research Center, MS 4840, Edwards, CA 93523, USA

(Received 6 February 1998, and in final form 11 September 2000)

Non-linear dynamics in aeroelastic systems are difficult to analyse and can induce unpredicted limit cycle oscillations in flight. This paper introduces wavelet analysis for processing flight data to extract information about structural non-linearities. Features and trends from wavelet transform maps of transient responses are used to detect and characterise polynomial non-linearities in stiffness. These features are also used to formulate functions that use transient responses at stable flight conditions to predict the onset of limit-cycle oscillations.

1. INTRODUCTION

Flight testing aircraft for envelope expansion is a dangerous and costly procedure because the onset of aeroelastic instabilities is often not predicted [1]. A limit-cycle oscillation (LCO) refers to a bounded periodic motion that is especially problematic. This motion is mathematically stable in the sense of Lyapunov but is effectively unstable for flight since it often leads to pilot injury and catastrophic damage to airframe components [2]. The F-16 demonstrates several well-known LCO behaviours when operating with particular store configurations [3]. The F/A-18 has also experienced an LCO for a particular store configuration [4]. Another LCO type of phenomenon was experienced by the B-2 when operating in a particular flight regime [5].

Several approaches have been formulated to analyse non-linearities and associated LCO using flight data. A common approach has been to estimate a model based purely on measured responses using system identification algorithms; however, these approaches typically have difficulties estimating low damped modes or lag terms associated with unsteady aerodynamics. A similar approach has been formulated that has shown success for predicting LCO [6]. This approach noted characteristics from wind tunnel measurements and identified model properties to match those characteristics [7]. The resulting model was not directly computed from flight data; however, it was formulated based on data observations.

Another approach that has been investigated is to utilise damping estimates to predict LCO. It has been noted that sensitivities in the instability predictions based on linear analysis have some correlation with the onset of LCO from non-linear dynamics [8]. This information was utilised to formulate neural network prediction functions that analyse flight data [9]. This information is also being considered in conjunction with a robust stability type of analysis that formally evaluated sensitivities [10].

Approaches based on alternative means of signal processing can be employed to consider LCO behaviours. Notably, wavelets provide a means of analysing time and frequency

0888–3270/01/020337 + 20 $35.00/0

content in data [11]. This type of processing decomposes the data into localised waveforms rather than the sum of infinite-length sinusoids that results from Fourier processing. Thus, wavelets naturally characterise features and patterns of size and time variation. Wavelets can be applied to the analysis of flight data through applications such as determining the linear modal characteristics of an aeroelastic system [12].

This paper considers wavelet analysis for processing response data from non-linear aeroelastic systems [13]. The time–frequency domain maps that result from wavelet transforms present information about localised periodicity that results from exciting the non-linearity [14]. Two applications are presented that consider free-decay responses of time-invariant systems that have non-linear polynomial stiffness functions.

One application that is presented in this paper is the use of wavelets to detect and characterise non-linearities. Several features and trends are seen in wavelet maps from transient responses that indicate the presence of non-linearities. Furthermore, these features and trends are exploited to describe the nature of the non-linearity. Such information can potentially be used to develop system identification algorithms in the time–frequency domain.

The other application presented in this paper is to use wavelets to predict the onset of an LCO. Responses at different operating points of a model are analysed to generate time–frequency maps. Functions based on properties of these maps are developed that extrapolate from stable conditions to the onset of an LCO.

A non-linear model of an aeroelastic testbed at Texas A&M University is used to demonstrate these applications [15]. Wavelet maps can detect and characterise different members from a class of structural non-linearities along with formulating LCO prediction functions. The results presented in this paper are only directly applicable to this particular system but the concepts may be extended to consider other classes of systems.

2. WAVELET ANALYSIS

2.1. WAVELETS AND THE WAVELET TRANSFORM

Wavelet analysis relies upon a family of basis functions, called wavelets, for signal processing in the time–frequency domain [16]. Wavelets are defined with respect to several mathematical properties such as square integrability and admissibility; however, they can be essentially considered as finite-duration waveforms for the limited purposes of this paper.

Each element, $\psi_{a,\tau}(t)$, of the family of wavelets used for analysis is written with respect to a mother wavelet $\psi(t)$. Essentially, the positive scalar a is used to stretch the wavelet and consequently increase the period and decrease the frequency components. Also, the scalar τ is used to shift the wavelet in time. Thus, the wavelet elements can be explicitly written in terms of the mother wavelet:

$$\psi_{a,\tau}(t) = \frac{1}{\sqrt{a}}\psi\left(\frac{t-\tau}{a}\right).$$

The wavelet transform is the tool used for wavelet analysis [11]. This transform is analogous in nature to the Fourier transform in which each process decomposes a signal into a sum of basis functions. The wavelet family is defined by the scalar parameters that represent scale and position; consequently, the wavelet transform results in a three-dimensional map. This map, $W(a, \tau)$, relates a measure of how much the signal, $x(t)$, correlates with $\psi_{a,\tau}(t)$ for each value of scale and position:

$$W(a,\tau) = \int_{-\infty}^{\infty} x(t)\psi^*_{a,\tau}(t)\,\mathrm{d}t.$$

The Morlet wavelet will be used throughout this paper. This mother wavelet is defined as an exponentially decaying sinusoidal signal. The software package used to generate the results use the following equation for the mother wavelet [17]:

$$\psi(t) = \mathrm{e}^{-(1/2)t^2} \cos 5t.$$

There are a multitude of wavelets that could be used; however, the Morlet wavelet is particularly attractive for analysing signals that are generated by dynamical systems. First, damped sinusoids are common responses from certain dynamical systems so it is natural to correlate these responses with Morlet wavelets. Second, the Morlet wavelet has a single frequency. If a signal correlates highly with a scaled Morlet wavelet, then the frequency of the wavelet indicates the frequency of some dynamic that generated the signal.

2.2. EXTRACTING INFORMATION FROM WAVELET MAPS

Wavelet analysis may seem more difficult to use than traditional Fourier analysis because it is difficult to interpret the wavelet parameters in terms of commonly understood concepts. For example, it is straightforward to identify a natural frequency from a spectral plot but this information is more difficult to identify on a wavelet map. An investigation of some wavelet properties will demonstrate that this type of useful information can indeed be extracted from wavelet maps.

A feature that can be easily extracted from a wavelet map is the dominant scale in the signal at each point in time. Consider a vertical strip, $W(A, \bar{\tau})$, taken from a three-dimensional map. This strip represents the correlations between the signal and wavelets that are centred at position $\bar{\tau}$ for all scale values given by the vector A. Define $\bar{W}$ as the peak magnitude of this correlation that occurs for the wavelet with scale of $\bar{a}$:

$$\bar{W} = W(\bar{a}, \bar{\tau}) = \max_{a \in A} W(a, \bar{\tau}) = \max_{a \in A} W(a, \tau)\Big|_{\tau = \bar{\tau}}.$$

The dominant scale, $\bar{a}$, is not identical to the concept of frequency; however, they can be closely related to the Morlet wavelet. Consider a given signal of frequency ω_{sig} which is sampled at a rate of f_{sig}. The wavelet map that is generated by analysing this signal will show a peak at the scale value of $\bar{a}$. This scale is determined by the frequency, ω_{wave}, and the sampling rate, f_{wave}, of the mother wavelet. Note that $f_{\mathrm{sig}} = 1000$, $f_{\mathrm{wave}} = 1$, and $\omega_{\mathrm{wave}} = 5$ rad/s $= 0.796$ Hz for the software used in this paper:

$$\bar{a} = \frac{f_{\mathrm{sig}}}{f_{\mathrm{wave}}} \frac{\omega_{\mathrm{wave}}}{\omega_{\mathrm{sig}}} = \frac{796}{\omega_{\mathrm{sig}}}.$$

The dominant scale can be used to identify the dominant frequencies at distinct times during the responses. These frequencies may correspond to natural frequencies of dynamics that dominate the response. The time-varying nature of the dominant scale can indicate that the properties of the dominant dynamics are changing during the response. In this way, a simple evaluation of the time–frequency wavelet map can reveal information about the system dynamics that goes beyond the information obtained from a spectral plot.

The concept of a dominant feature is related to the concept of a ridge that has been developed for analysing wavelet maps [18]. These ridges are defined by stationary points of instantaneous frequency and are used to define a skeleton that describes dominant parts of a signal. These ridges and skeletons have been used to analyse responses from non-linear systems and note properties of the dynamics [19, 20]. The ridge is a more rigorous mathematical approach than the concept of dominant scale presented here; however, the simple approach is sufficient for the purposes of this paper.

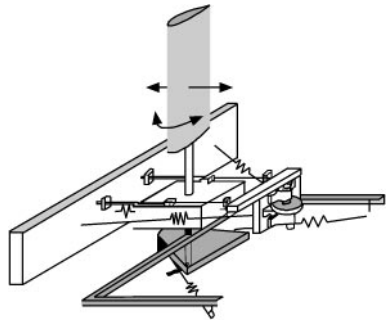

Figure 1. Texas A&M University Aeroelastic Testbed.

TABLE 1

Model parameters

m	12.387	c_y	27.43
b	0.135	c_α	0.036
I_α	0.065	k_y	2844.4
ρ	1.225	c_{l_α}	6.28
x_α	0.2467	e	− 0.6

3. NON-LINEAR AEROELASTIC MODEL

Responses of a non-linear aeroelastic model will be analysed in this paper. The model describes a testbed that has been developed at Texas A&M University for flutter research [15]. The testbed allows pitch and plunge motions of a wing section that represent typical bending and torsion motions of aeroelastic wings. Non-linearities are introduced through a series of springs and cams in the support structure for the wing as shown in Fig. 1.

Consider the aeroelastic equations of motion for this pitch–plunge system:

$$\begin{bmatrix} m & mx_\alpha b \\ mx_\alpha b & I_\alpha \end{bmatrix} \begin{bmatrix} \ddot{y} \\ \ddot{\alpha} \end{bmatrix} + \begin{bmatrix} c_y & 0 \\ 0 & c_\alpha \end{bmatrix} \begin{bmatrix} \dot{y} \\ \dot{\alpha} \end{bmatrix} + \begin{bmatrix} k_h & 0 \\ 0 & k_\alpha \end{bmatrix} \begin{bmatrix} y \\ \alpha \end{bmatrix} = \begin{bmatrix} -L \\ M \end{bmatrix}.$$

The states of the system are y for the plunge position and α for the pitch angle. Other variables include the air velocity U, the non-dimensional distance between the elastic axis and the centre of mass x_α, the location of the elastic axis e, the mass of the wing m, the mass moment of inertia I_α, semichord length b, structural damping coefficients in pitch and plunge c_y and c_α, and spring stiffness k_y and k_α. The lift L and moment M per unit span are determined by quasi-steady aerodynamic theory using the lift coefficient c_{l_α}:

$$L = \rho U^2 b c_{l_\alpha} \left(\alpha + \left(\frac{1}{2} - e \right) \frac{b}{U} \dot{\alpha} + \frac{1}{U} \dot{y} \right)$$

and

$$M = (\tfrac{1}{2} - e)\, bL.$$

Values of the parameters used for this study are given in Table 1.

Non-linearities are introduced into the system dynamics through the stiffness associated with pitch movement. This stiffness, k_α, is described by a non-linear polynomial function

of the pitch angle. Such structural non-linearities occur in physical aeroelastic systems and have been investigated to determine their effect on inducing limit-cycle oscillations [21].

4. DETECTING AND CHARACTERISING NON-LINEARITIES

4.1. MODEL PROPERTIES

Models of the Texas A&M aeroelastic system are formulated using three types of stiffness functions to investigate a variety of behaviours related to different non-linearities. The stiffness functions associated with the pitch degree of freedom are chosen to represent a linear spring, a non-linear hardening spring, and a non-linear softening spring. Each of these functions is a polynomial function of the pitch angle.

The linear spring constant is denoted by $k_\alpha = k_{\text{lin}}$:

$$k_{\text{lin}} = 2.82.$$

A softening spring will be considered for analysis in the model. A softening spring has the property that its restoring moment is less than the moment from a linear spring for large values of pitch angle. The softening spring function is denoted by $k_\alpha = k_{\text{soft}}$:

$$k_{\text{soft}} = 2.82 - 200\alpha^2 + 10\,000\alpha^4.$$

A hardening spring will also be considered for analysis in the model. A hardening spring has the property that its restoring moment is greater than the moment from a linear spring for large values of pitch angle. The hardening spring function is denoted by $k_\alpha = k_{\text{hard}}$:

$$k_{\text{hard}} = 2.82 - 62.3\alpha + 3709.7\alpha^2 - 24196.0\alpha^3 + 48757\alpha^4.$$

The restoring moment resulting from each spring is shown in Fig. 2. This plot shows the softening and hardening behaviours as compared to the linear behaviour for a limited range of pitch angles. The asymmetry of the hardening spring is somewhat difficult to see on this plot; however, there is a definite asymmetry resulting from terms involving odd powers of α that becomes more noticeable as pitch angle increases.

Note that the softening spring actually becomes a hardening spring for magnitude of pitch angles greater than 0.15 rad. The analysis in this paper will only be focusing on pitch angles less than this magnitude, so k_{soft} will always be treated as softening.

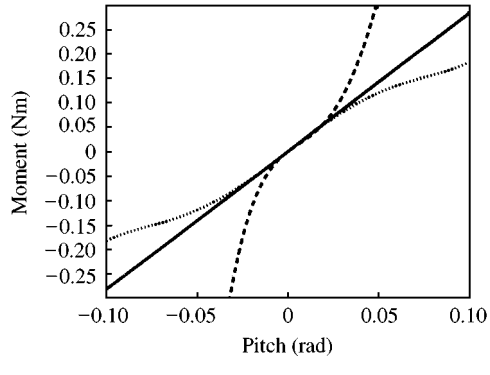

Figure 2. Spring reaction moment for different pitch angles: linear (—); softening (. . .); hardening (– – –).

TABLE 2

Model properties of the linearized aeroelastic model at airspeeds, U, in m/s

	$U = 4$	$U = 6$	$U = 8$	$U = 10$	$U = 11.9$
ω_y (Hz)	2.73	2.67	2.54	2.36	2.00
ω_α (Hz)	1.09	1.17	1.29	1.48	1.86
ζ_y	0.086	0.087	0.089	0.094	0.171
ζ_α	0.053	0.057	0.060	0.059	− 0.014

The models with each of these springs can be linearised around the equilibrium condition at $\alpha = 0$. The system dynamics of these linear models will be identical because the different spring functions are identical when the terms involving α are eliminated. Thus, the systems at stable flight conditions should behave similarly with nearly identical natural frequencies for responses with small α values. The natural frequencies and dampings associated with the pitch and plunge modes of the linearised models at different airspeeds are given in Table 2.

A classical flutter instability is encountered for the linearised dynamics at $U = 11.9$ m/s. This instability is caused by a coupling of the pitch and plunge modes. As the natural frequencies coalesce, the damping of the plunge mode increases while the damping of the pitch mode decreases. The linearised models do not predict any instabilities or limit-cycle oscillations for lower airspeeds.

4.2. SIMULATED RESPONSES

Simulated responses are computed for each non-linear model at an airspeed condition of $U = 8$ m/s. The responses simulate free decay behaviour of the system to initial conditions given at $t = 0$:

$$y(t = 0) = 0.01 \text{ m}, \qquad \dot{y}(t = 0) = 0 \text{ m/s}$$

$$\alpha(t = 0) = 0.1 \text{ rad}, \qquad \dot{\alpha}(t = 0) = 0 \text{ rad/s}.$$

Figure 3 presents the pitch angle responses and Fig. 4 presents the plunge responses.

Time-scale information is obtained by computing the continuous wavelet transform of these time responses. The plunge response decays quickly to zero and so the wavelet transforms for this data will not be presented. The pitch response remains significant even after the plunge motion has decayed so this data will be used for analysis. Figure 5 presents the maps generated by a wavelet analysis on the pitch data using real Morlet wavelet basis functions.

Figure 5 shows two-dimensional representations of the three-dimensional wavelet maps. The correlation magnitude between the signal and wavelets at each position and scale value is represented by a shade of gray with white implying low correlation and black implying high correlation. Such a shading approach may not be optimal because several closely spaced scales will often appear to have a similar correlation magnitude and the resulting signal decomposition appears to be spread over these scales; however, the three-dimensional images are often more difficult to display.

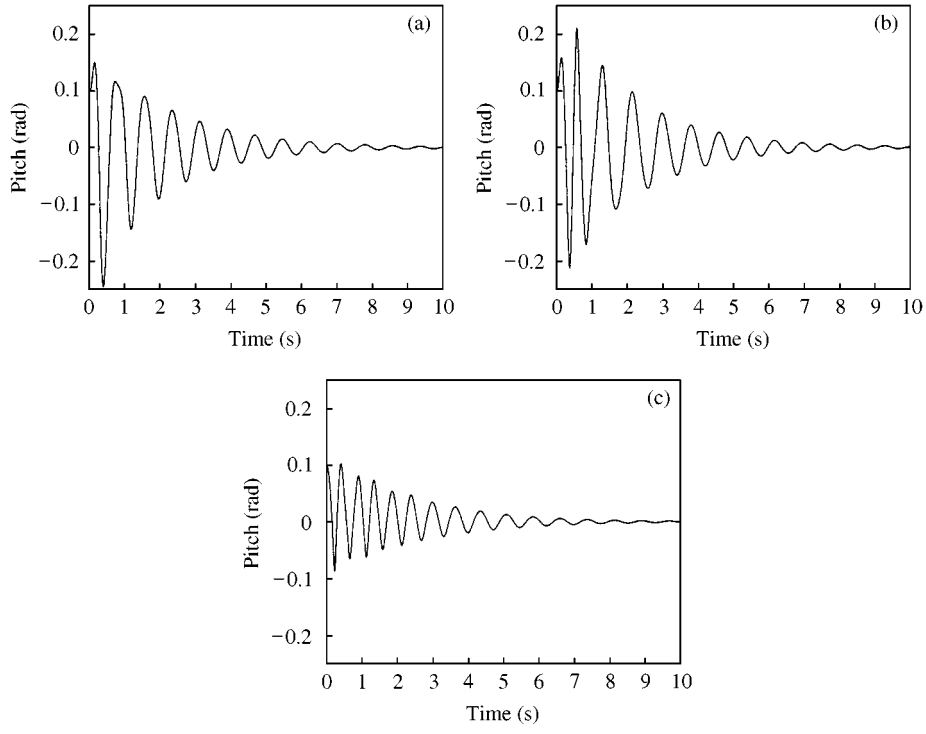

Figure 3. Simulated responses of the pitch angle at $U = 8$ m/s: model with k_{lin} (a); model with k_{soft} (b); model with k_{hard} (c).

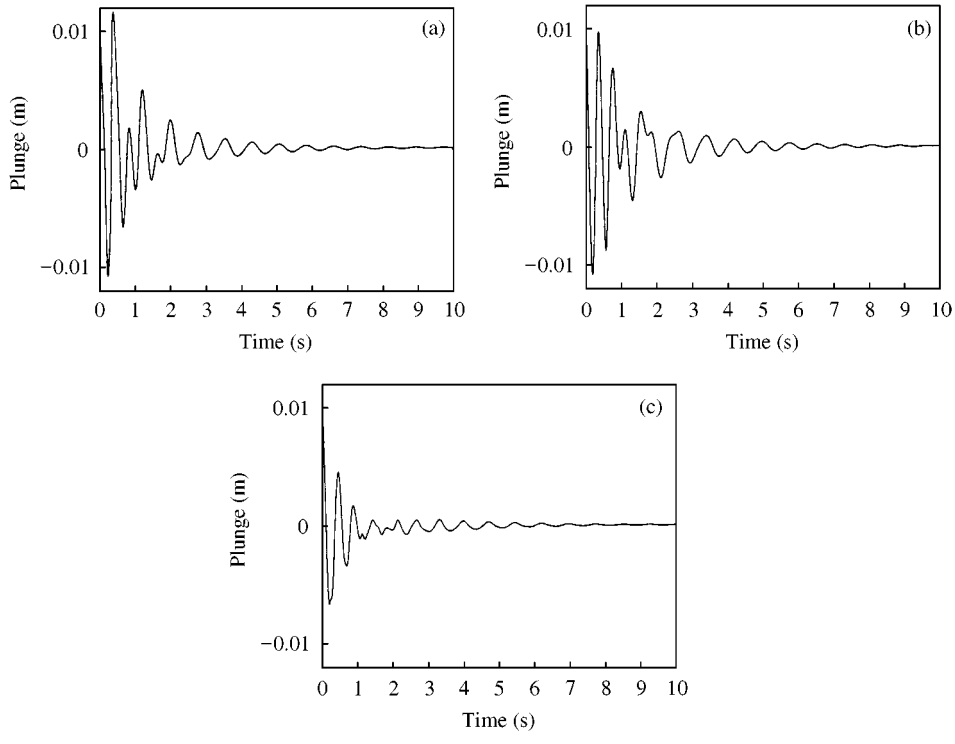

Figure 4. Simulated responses of the plunge displacement at $U = 8$ m/s: model with k_{lin} (a); model with k_{soft} (b); model with k_{hard} (c).

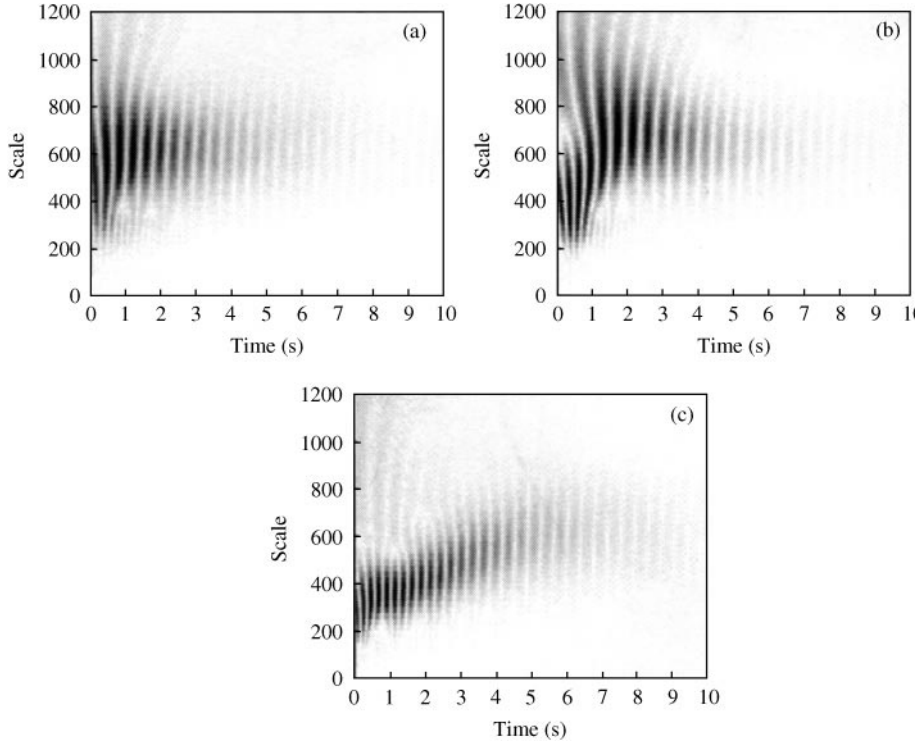

Figure 5. Wavelet transform maps of the pitch data: model with k_{lin} (a); model with k_{soft} (b); model with k_{hard} (c).

The analysis of Fig. 5 may be simplified by extracting information about the dominant features. The time-varying feature of dominant scale for the wavelet maps is shown in Fig. 6. These dominant scales indicate the scale associated with the wavelet that had largest correlation with the signal.

Define regions of time intervals to simplify the following discussions about analysing the wavelet maps:

$$\text{Region I} \quad 0 < t < 2\,\text{s}$$

$$\text{Region II} \quad 2 < t < 7\,\text{s}$$

$$\text{Region III} \quad 7 < t < 10\,\text{s}.$$

4.3. DETECTING NON-LINEARITIES

The time responses and associated wavelet maps demonstrate clear differences in the nature of each response. These plots may not be immediately obvious to interpret; however, a careful examination reveals that the wavelet analysis presents information which can be directly compared to properties of the dynamical systems.

The issue of detecting non-linearities will be addressed under several assumptions. First, the response will be assumed to have been generated from a single-mode system. Additionally, that system will be assumed to be time invariant. A further assumption will be that the responses are generated by free-decay motion with no external forcing.

The assumption of a single-mode system will cause the analysis to ignore any data contained in Region I. This initial portion of the response is highly transitory. The plunge

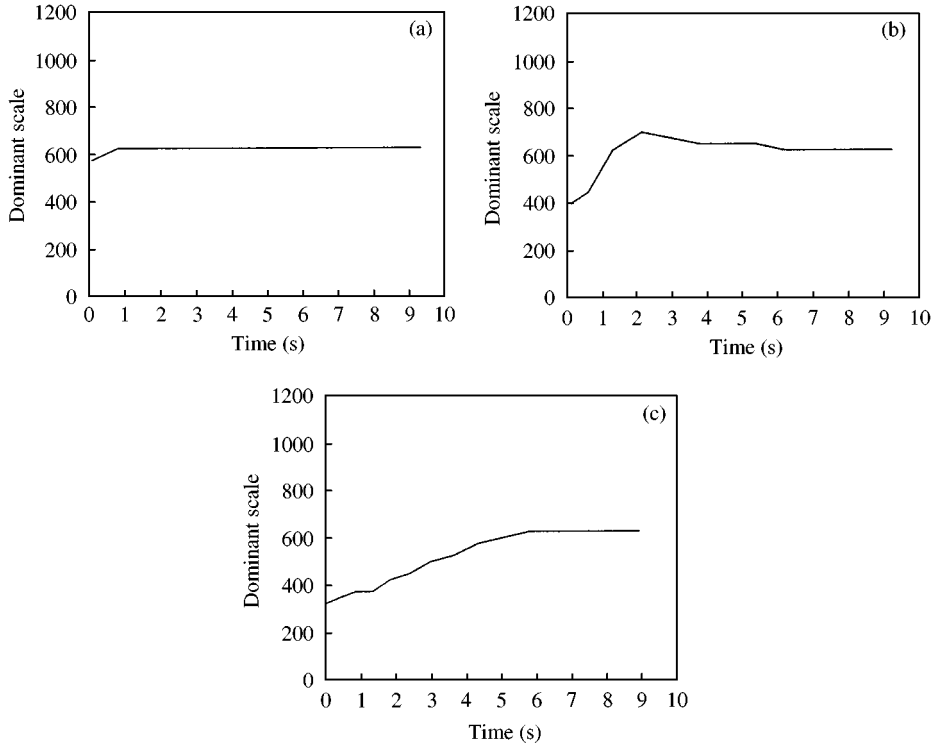

Figure 6. Dominant scales associated with the pitch data: model with k_{lin} (a); model with k_{soft} (b); model with k_{hard} (c).

motion is quite noticeable and does not damp out until the beginning of Region II. In particular, note that the small scales, or equivalently high frequencies, that dominate this portion correlate more to the natural frequency of the plunge mode than the pitch mode. Thus, the initial response contains large components from both modes and so will not be considered.

The response during Region II is a valid data that may be considered without grossly violating the assumptions. Note that the plunge motion is quite small after $t = 2$ s whereas the pitch motion is still reasonably large. This implies the response is essentially due to the single-pitch mode.

The behaviours of the responses throughout Region II are dramatically different. These behaviours are most easily analysed by considering the dominant scale associated with each response. The time variation of the dominant scale can be used to indicate the presence of a system non-linearity.

The constant value of the dominant scale for the linear system response is directly indicative of linear system dynamics. Consider that the free-decay response from a linear and time-invariant single-mode system should be an exponentially decaying sinusoid with constant frequency. Consequently, the dominant scale associated with that response should be constant. The scale in Fig. 6(a) demonstrates this nature.

Furthermore, the value of the dominant scale associated with the response in Fig. 6(a) is $\bar{a} = 625$. This corresponds to a frequency of $\omega = 1.27$ Hz. Thus, the wavelet map indicates the response is from a linear system and that the natural frequency of that linear system is near 1.27 Hz.

The time-varying value of the dominant scale can thus be used to detect non-linearities. The responses are seen to be essentially associated with a single-mode dynamic and clearly there is no additional forcing functions. The time-varying nature of the dominant scale can only result from a time-varying linear system or a time-invariant non-linear system. If the assumption of time invariance is made, then the wavelet maps in Fig. 6(b) and (c) clearly indicate the effect of non-linearities.

4.4. CHARACTERISING NON-LINEARITIES

The wavelet maps can be used to detect non-linearities; however, some further analysis will demonstrate that they can also be used to characterise those non-linearities. This characterisation will indicate the general nature of the non-linearity and imply some of its properties.

There are several assumptions that will be made for this analysis. Certainly, the basic assumptions associated with detecting non-linearities, such as time-invariant single-mode systems, will be required. Additionally, it will be assumed that the non-linearities occur only in the stiffness parameters. These non-linearities will be limited to polynomial functions of pitch angle. Of course, these assumptions are quite restrictive; however, this paper is intended to present the basic concepts rather than any type of generalised solutions.

Consider the nature of responses from a system whose polynomial non-linearity implies a hardening spring stiffness. This spring will incur a larger restoring moment than a linear spring when the pitch angle is large. Correspondingly, the response of the non-linear system will return to the origin sooner than the response of the linear system. Thus, the sinusoidal response will have a shorter period and a higher frequency for the non-linear system than for the linear system.

The dominant scale feature associated with the Region II response in Fig. 6(c) demonstrates the properties associated with a hardening spring. Namely, the dominant scale is initially small and continually increases throughout this time interval. This feature is equivalent to a frequency that is initially large but decreases as the response continues. This plot can be correlated with the time-domain response of Fig. 3(c) which shows that the pitch angle is initially large but decreases as time progresses. In essence, the effect of the non-linearity is decreasing so the frequency of the response should be decreasing. Thus, the wavelet map indicates that the system has a hardening spring stiffness.

Similarly, consider the nature of responses from a system whose polynomial non-linearity implies a softening spring stiffness. This spring will incur a smaller restoring moment than a linear spring when the pitch angle is small. Correspondingly, the response of the non-linear system will take longer to return to the origin than the response of the linear system. In this way, the sinusoidal response will have a longer period and lower frequency for the non-linear system than for the linear system.

Analysing the dominant scale feature in Fig. 6(b) indicates that the associated response is generated by a system with a softening spring. This feature, in Region II, shows the dominant scale is initially large and decreases throughout the time interval. The frequency associated with the response can thus be noted as being small but increasing as time increases. Correspondingly, the time response in Fig. 3(b) shows that the pitch angle is decreasing, and the effect on non-linearity is decreasing, as the response progresses. Thus, the wavelet map indicates that the system has a softening spring stiffness.

Some insight into the nature of the non-linearity can also be found by continuing the analysis into Region III of the responses. Namely, the dominant scales associated with the non-linear responses are gradually varying throughout Region II until reaching and maintaining a constant value throughout Region III. This constant value of $\bar{a} = 625$ is the same for the response from the system with either hardening or softening spring.

Furthermore, it implies a frequency of around 1.27 Hz and matches the natural frequency of the pitch mode of the linear model.

This gradual change from large or small frequencies to the linearised natural frequency indicates that the assumption of polynomial non-linearities is not invalid. There are no dramatic shifts in the nature of the time-varying dominant scale so the non-linearity must be a relatively smooth and well-behaved function of the gradually decreasing pitch angle. This would be expected from a polynomial function rather than from, for example, a discontinuous non-linearity.

Also, the final value of the dominant scale implies there is no constant bias. Essentially, the effect of the non-linearity is nullified for small pitch angles because the dominant scale is identical for the Region III responses of either the linear or non-linear systems.

The nature of the time-varying value of the dominant scale can thus be used to characterise non-linearities. The increasing or decreasing behaviour indicates that the stiffness is either hardening or softening. Furthermore, the smooth transition of these values to the value of dominant scale from the linearised responses indicates that the polynomial is somewhat smooth and well-behaved with no constant bias term.

4.5. LIMITATIONS

The analysis in this section demonstrates that wavelet maps and dominant scales corresponding to peaks in the wavelet maps may be used to detect non-linearities from response data of an aeroelastic model. The time-varying behaviour of the dominant scales indicates that a non-linearity is present in the system. Furthermore, the nature of that time-varying behaviour indicates properties of the non-linearity.

It is important to note that there were several restrictive assumptions made in this section that enabled the wavelet transforms to be so effective in detecting and characterising non-linearities. It was always assumed the analysis considered the free-decay response data from a single mode of a time-invariant system. The time-varying scale for such data could only be caused by a non-linearity since linear systems theory would preclude such a time-varying response frequency from a time-invariant system.

This paper makes no general claims about the ability of wavelets to detect non-linearities when analysing data that violates the assumptions. Example systems could be formulated in which a forced response of a linear time-invariant system could generate wavelet maps similar to Fig. 5. Example systems could also be generated in which the free-decay response of a linear time-varying system could generate these wavelet maps. Therefore, the wavelet analysis presented here is only immediately applicable to systems which are similar in nature to the particular model under investigation.

5. PREDICTING LIMIT CYCLE BEHAVIOUR

5.1. MODEL PROPERTIES

Wavelet analysis can be considered for predicting limit cycle oscillations by investigating responses of a non-linear system for a range of variables in the parameter space. The aeroelastic model is used for this by generating responses at increasing airspeeds until a bifurcation point is reached. The analysis will be restricted to considering responses from the model with the hardening spring, k_{hard}, for this detailed analysis:

$$k_{\text{hard}} = 2.82 - 62.3\alpha + 3709.7\alpha^2 - 24196.0\alpha^3 + 48757\alpha^4.$$

The aeroelastic system with this spring function experiences a Hopf-type bifurcation at $U = 9.8$ m/s airspeed [22]. This type of bifurcation is characterised by a significant change

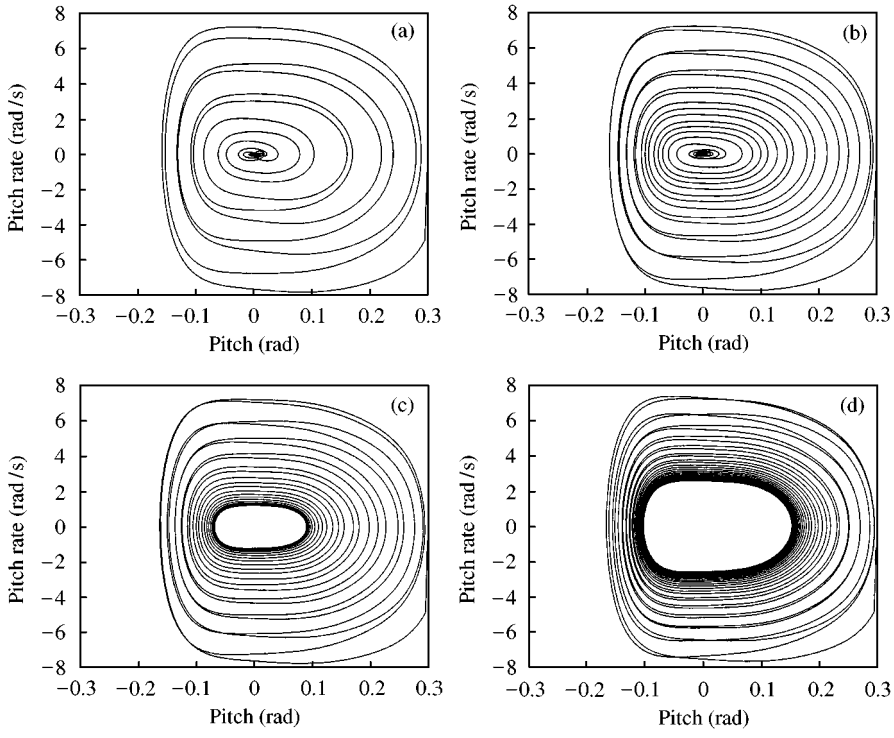

Figure 7. Phase plane plots of pitch rate (rad/s) *vs* pitch (rad) for simulated responses of the model with the non-linear hardening spring: $U = 4.0$ m/s (a); $U = 9.0$ m/s (b); $U = 10.0$ m/s (c); $U = 12.0$ m/s (d).

in the attracting sets between airspeeds lower and higher than the bifurcation point [23]. The system has an attracting set consisting of a single stable point at the origin, $\alpha = \dot{\alpha} = 0$ and $y = \dot{y} = 0$, for low airspeeds. The attracting set for airspeeds above the bifurcation has changed to a stable periodic orbit with the origin becoming an unstable point so that all trajectories are attracted to the orbit and a limit cycle is induced.

The stability properties and attracting sets can be visualised by computing time responses of the non-linear mode at different airspeeds [24]. Each response is a free-decay response at a constant airspeed with initial conditions given at time $t = 0$:

$$y(t = 0) = 0.0 \text{ m}, \qquad \dot{y}(t = 0) = 0 \text{ m/s}$$

$$\alpha(t = 0) = 0.3 \text{ rad}, \qquad \dot{\alpha}(t = 0) = 0 \text{ rad/s}.$$

Figure 7 plots the phase plane of pitch rate against pitch for the measured responses at four airspeeds. The trajectories for the airspeeds of $U = 4.0$ and 9.0 m/s, which are lower than the bifurcation airspeed, decay to the stable attracting origin. The trajectories for the airspeeds of $U = 10.0$ and 12.0 m/s, which are greater than the bifurcation airspeed, demonstrate the periodic attracting set which generates the limit-cycle oscillation.

The responses and the periodic attracting limit cycles have several interesting features that should be noted. One feature is the asymmetry of each trajectory and limit cycle. This feature is expected because the hardening spring is asymmetric about the pitch angle so the restoring moment is greater for negative pitch angles than for positive pitch angles. Thus, the system response is skewed towards positive pitch angles. Another feature is the increasing number of spirals until the trajectory settles to an attracting set. This feature is

caused by a decrease in damping as airspeed increases. Thus, the transient response takes more time to decay and results in more spirals until an attracting set is reached.

5.2. DOMINANT FEATURES

Wavelets maps are computed for the simulated pitch angle responses. These maps, which are computed by using Morlet wavelets as basis functions, are presented in Fig. 8.

Several features and trends can be noted from a qualitative analysis and visual inspection of Fig. 8. One immediate obvious feature is the high correlation for small-scale wavelets with the initial responses. This feature indicates the response begins with a frequency above 8 Hz and transitions to a frequency near 4 Hz after 2 s. This feature is partly caused by coupling with the plunge mode; however, the main cause is the non-linearity in the pitch mode. The large initial condition causes the non-linearity to be strongly excited. Thus, the response from the hardening spring has a frequency that is much higher than that of a linear spring until the response decays.

Another immediate obvious feature is the change in scale after a few seconds for the responses at low airspeeds. Note that at $U = 1$ and 2 m/s there are distinct shaded regions in the wavelet maps. The initial responses show large correlation with small-scale wavelets but the later responses show large correlation with large-scale wavelets. More importantly, there seems to be a sharp disconnect between these shaded regions. This behaviour remains as airspeed increases with the discontinuity occurring at later times and with smaller magnitude.

The feature associated with the discontinuity in scales alters for airspeeds greater than 8 m/s. The shaded regions for these responses appear to be smoothly connected. There is still a transition between the shaded regions; however, there are no discontinuities. It is interesting to note that this transition, similar to the discontinuity at low airspeeds, decreases in magnitude and occurs at later times as the airspeed increases.

Figure 9 presents the dominant scale as a function of time for each different airspeed. These functions contain only the dominant information of Fig. 8 and thus are easier to analyse than the wavelet maps. In particular, the discontinuities and transitions at each airspeed are easy to recognise. Note that there is clearly a decrease in magnitude and increase in position associated with the largest change in dominant scale.

5.3. FUNCTION TO PREDICT LCO

The transition between dominant periodicity in the responses presents several characteristics that may be exploited to predict the onset of LCO. The main properties of the transition are the smoothness and magnitude of the change from low to high dominant scales along with the time position at which this change occurs. These properties can be determined by computing the derivative with respect to time of the dominant scales. The derivatives, which are shown in Fig. 10, formally represent the transitions and changes in scale.

The derivative information in Fig. 10 provides a quantitative description of the transition from a dominant low-scale waveform to a high-scale waveform in the response data. The magnitude of the jump during this transition is clearly seen to be large for the responses at low airspeeds and decreasing as the airspeed increases. Also, the time position at which the largest jump occurs is seen to increase as the airspeed increases. These two features which combine to signify the transition from a dominant low-scale waveform to a high-scale waveform becomes smoother and delayed as the airspeed increases towards the bifurcation point.

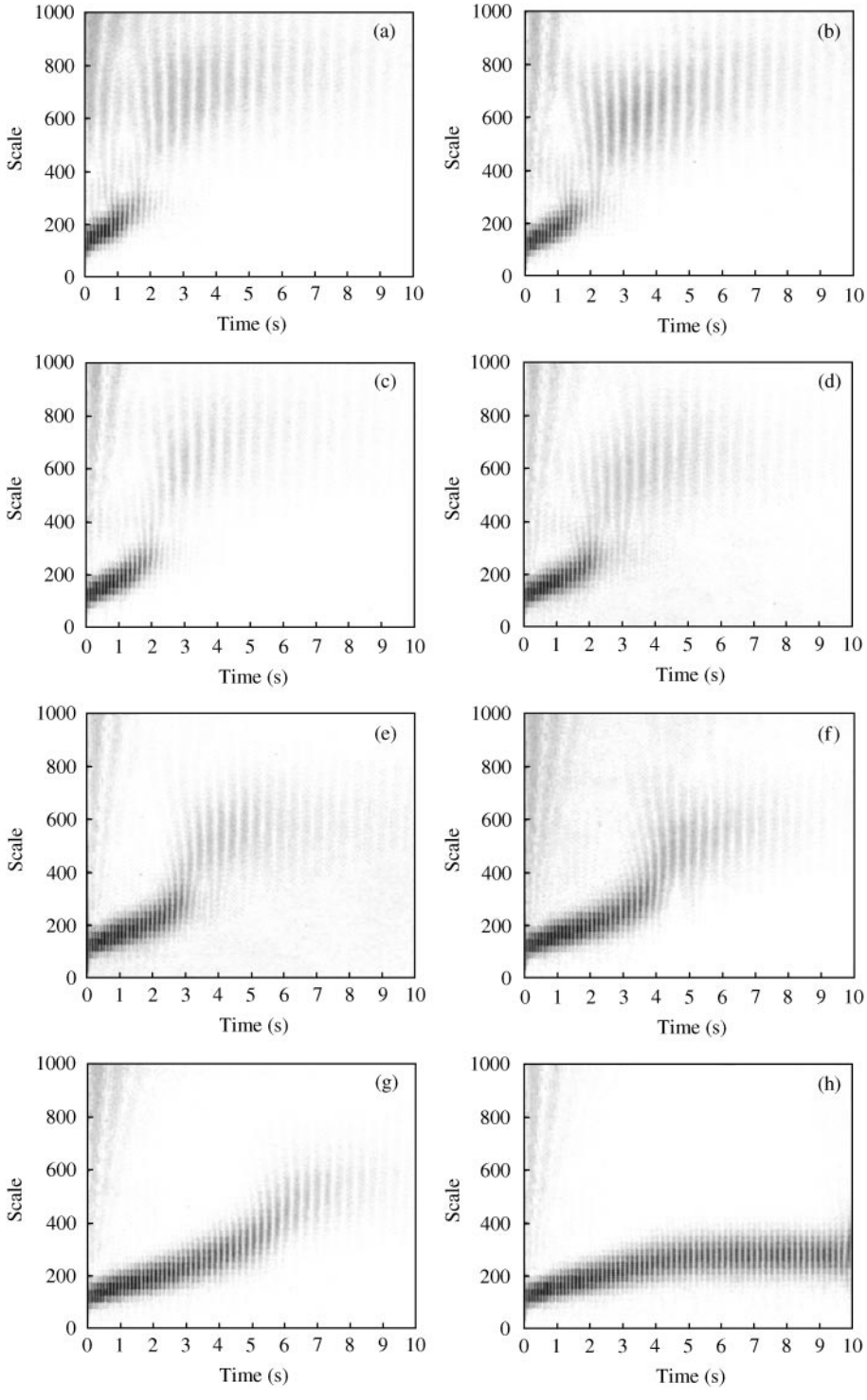

Figure 8. Wavelet transform maps of the pitch data at different airspeeds: $U = 1.0$ m/s (a); $U = 2.0$ m/s (b); $U = 4.0$ m/s (c); $U = 6.0$ m/s (d); $U = 8.0$ m/s (e); $U = 9.0$ m/s (f); $U = 9.5$ m/s (g); $U = 10.0$ m/s (h).

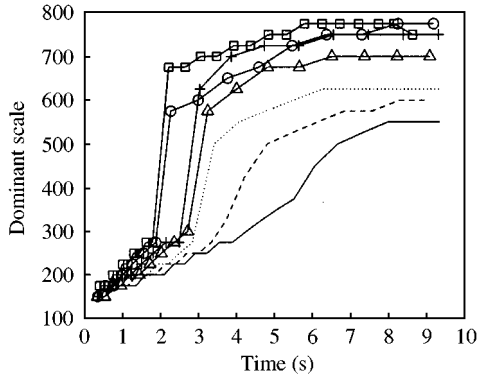

Figure 9. Dominant scale associated with the pitch data at different airspeeds: $U = 1.0$ m/s (□); $U = 2.0$ m/s (○); $U = 4.0$ m/s (+); $U = 6.0$ m/s (△); $U = 8.0$ m/s (...); $U = 9.0$ m/s (---); $U = 9.5$ m/s (—).

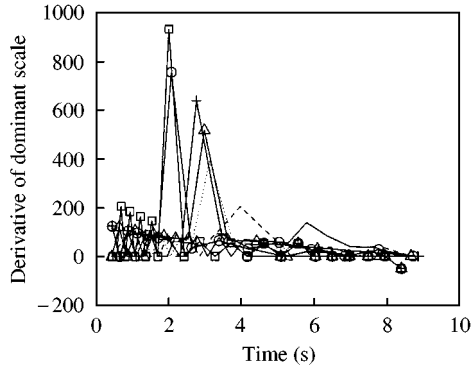

Figure 10. Derivative of dominant scale at different airspeeds: $U = 1.0$ m/s (□); $U = 2.0$ m/s (○); $U = 4.0$ m/s (+); $U = 6.0$ m/s (△); $U = 8.0$ m/s (...); $U = 9.0$ m/s (---); $U = 9.5$ m/s (—).

The interesting features of Fig. 10, namely the magnitude and time of the peak derivative of the dominant scale functions, can be extracted to focus on this information. Define parameters $\Delta_{\bar{a}}$ and $t_{\bar{a}}$ such that the derivative of $\bar{a}$ achieves its maximum value of $\Delta_{\bar{a}}$ when evaluated at $t_{\bar{a}}$. These parameters are functions of airspeed since different $\Delta_{\bar{a}}$ and $t_{\bar{a}}$ correspond to responses from different airspeeds:

$$\Delta_{\bar{a}} = \left.\frac{\mathrm{d}\bar{a}}{\mathrm{d}t}\right|_{t=t_{\bar{a}}} = \max_{\tau} \left.\frac{\mathrm{d}\bar{a}}{\mathrm{d}t}\right|_{t=\tau}.$$

Figure 11 presents the values of $\Delta_{\bar{a}}$ as they vary with airspeed. The curve is computed with seven points corresponding to the seven airspeeds used to compute the derivative functions in Fig. 10. This plot clearly shows the decrease in magnitude of the peak derivative of the dominant scale as the airspeed is increased.

Figure 12 presents the times, $t_{\bar{a}}$, at which the responses demonstrate the largest change in dominant scale. These times correspond to the peak derivative values from Fig. 11. This plot clearly shows the time at which the transition from a low to a high dominant scale occurs is delayed as the airspeed is increased.

The information from Figs. 11 and 12 suggests a relationship that may be used to formulate a limit cycle prediction function. There are several desired properties this function

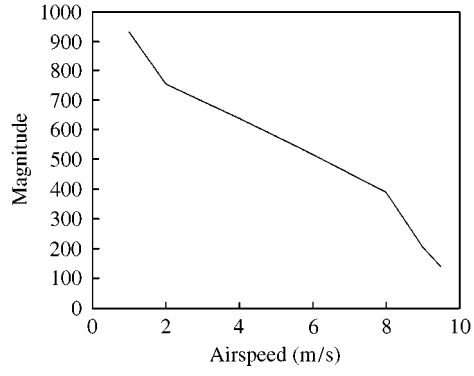

Figure 11. Variation of $\Delta_{\bar{a}}$ with airspeed.

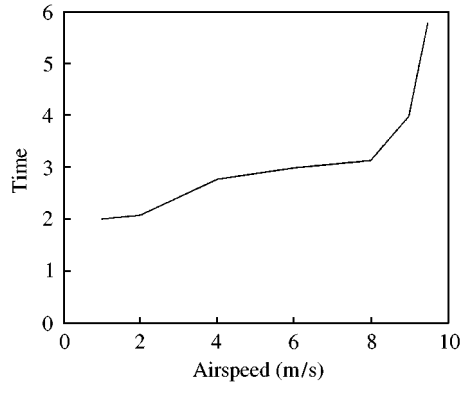

Figure 12. Variation of $t_{\bar{a}}$ with airspeed.

should have such as being smooth and well behaved. This property ensures that the function avoids any sharp non-linearities that prevent accurate extrapolation from stable to unstable flight conditions. Another desired function property is linearity. Non-linear functions are sometimes used as prediction functions; however, non-analytic methods based on extrapolation usually work best with linear functions. Also, this function should have a well-defined terminus condition that clearly indicates the onset of a limit cycle.

A prediction function, $\phi_{\bar{a}}$, can be formulated from the wavelet transform information by dividing the $\Delta_{\bar{a}}$ values from Fig. 11 with the $t_{\bar{a}}$ values from Fig. 12:

$$\phi_{\bar{a}} = \frac{\Delta_{\bar{a}}}{t_{\bar{a}}}.$$

This function should be an acceptable prediction function and have the desired properties. The variation of $\phi_{\bar{a}}$ with airspeed should be relatively smooth and well behaved since both $\Delta_{\bar{a}}$ and $t_{\bar{a}}$ are smooth and well behaved. $\phi_{\bar{a}}$ will have some degree of linearity since the rate of change of the decreasing $\Delta_{\bar{a}}$ values is similar to the rate of change of the increasing $t_{\bar{a}}$ values. Also, there is a well-defined terminus condition of $\phi_{\bar{a}} = 0$ for the airspeed at which a limit cycle is encountered. This condition arises because any transition between dominant scales for a limits cycle response is smooth and delayed so $\Delta_{\bar{a}}$ is small while $t_{\bar{a}}$ is large causing $\phi_{\bar{a}} \approx 0$. The derived values of $\phi_{\bar{a}}$ are given in Fig. 13.

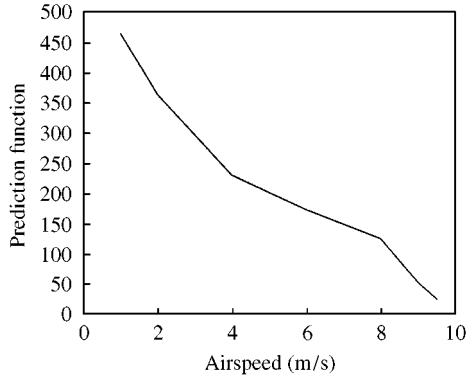

Figure 13. Prediction function $\phi_{\bar{a}}$.

A linear analytical function ϕ can be computed from an optimal curve fit to the simulated values of $\phi_{\bar{a}}$:

$$\phi = -47U + 468.$$

This function is computed using responses from airspeeds ranging up to the onset of a limit cycle so it logically predicts LCO near the correct unstable airspeed $U = 9.8$ m/s; however, such a large amount of information is not necessary. The near linearity of $\phi_{\bar{a}}$ in Fig. 13 indicates a function ϕ could be computed using only responses at airspeeds well below the instability. For example, an optimal linear curve fit of $\phi_{\bar{a}}$ from airspeeds $U = \{2, 4, 6\}$ m/s produces a function ϕ that predicts the onset of a limit cycle at an airspeed which is within 5% of the true value. Thus, the wavelet transform provides information about this system that can predict a limit cycle from response at a limited range of stable flight conditions.

The ability to formulate an accurate predictor function like ϕ is an almost optimal situation for experimental testing; however, the individual properties of $\Delta_{\bar{a}}$ and $t_{\bar{a}}$ functions should also be monitored. The $\Delta_{\bar{a}}$ parameter increases and the $t_{\bar{a}}$ parameter decreases near the instability so a threshold test on their values could be used to indicate the proximity to a limit cycle. Also, each parameter is nearly linear until flight regions close to a bifurcation so another test on the linearity of their behaviour could be used to indicate the proximity to a limit cycle. These tests are basically stability indicator tests, rather than stability predictor tests, but they provide additional information which can augment traditional stability indicators such as damping ratios and any experimental stability predictor functions such as ϕ. The combination of these different types of information may decrease errors in stability estimates caused by noise, unobserved dynamics, and non-repeatability.

5.4. LIMITATIONS

The approach adopted to formulate ϕ in Fig. 13 utilises local properties of the response data to determine suitable coefficients for the function. This approach is not based on analytical properties of the dynamics and there may not be an obvious physical interpretation of the resulting function; however, this type of approach is often the only useful method. Analytical solutions do not exist for many non-linear differential equations which describe dynamical systems so experimental testing must be used to determine characteristics and properties. Indeed, one of the few functions which can accurately predict the onset of a limit cycle for a particular system is a fourth-order polynomial that was developed by observing system responses [25]. This polynomial is formulated from a curve fit algorithm using

localised frequency properties computed from experimental data and is therefore conceptually analogous to the localised periodicity properties used to compute ϕ.

There is more information besides the time and magnitude of dominant scale transitions associated with the pitch response data that can be utilised to formulate stability indicators and prediction functions. The peak magnitude of the correlation between the signal and the wavelets can be interpreted as a measure of energy in the signal so its decay rate and other trends may indicate properties of the non-linear dynamics. Also, the same procedures used to develop ϕ from pitch response data can be used to develop prediction functions from the plunge response data.

There are several aspects associated with the response data that have not been considered in the formulation of ϕ that should be investigated in future research. The main property of the wavelet maps that was used to develop this function is the transition from a dominant low-scale periodicity to a dominant high-scale periodicity in the response data. One aspect of the response that may greatly affect this transition is the initial conditions used to begin the free-decay motion. Initial conditions with a small magnitude will not strongly excite the non-linearity so it seems improbable that information of a transition could be detected with the wavelet transforms.

Another issue that may be important is the desire to formulate a linear prediction function. The data in Fig. 13 may actually be better fit with a higher-order polynomial. Such an approach was not considered for this paper but it may be of interest for future research.

6. APPLICABILITY TO GENERAL NON-LINEAR SYSTEMS

This paper presents results that are directly applicable to a specific system and may not be useful for general non-linear systems. These results are formulated by exploiting dynamical properties of the Texas A&M University aeroelastic wind tunnel system with a polynomial stiffness function. Formulating similar results for a general class of non-linear systems would require evaluating dynamical properties specific to that class.

The detection and characterisation of non-linearities is accomplished using wavelet transform maps because of several strong assumptions. These assumptions require response data to be generated from a free decay of time-invariant dynamics which are dominated by a single mode. Additionally, the non-linearity in the dynamics is assumed to affect the stiffness. Methods of detection and characterisation of non-linearities have been developed for non-linear systems which violate these assumptions but properties other than those presented in this paper will need to be investigated.

The prediction function is formulated for the Texas A&M University system with a particular non-linear polynomial stiffness function and generally would not be accurate for other systems. The order and coefficients of this function would need to be altered to reflect the properties of a different dynamical system.

There are no guarantees that this wavelet approach will be of any use for different systems; however, the underlining methodology is general and not specific to any type of model. The wavelet-based approach can be utilised with a different class of systems to derive new properties for detecting and characterising non-linearities and to formulate new functions for predicting the onset of a limit cycle. This approach can be considered for future investigation of many classes of non-linear systems with behaviours including hysteresis and free play along with different structural and aerodynamic non-linearities.

7. CONCLUSION

This paper develops a methodology to analyse non-linear dynamical systems by utilising wavelet transforms. Responses from an aeroelastic model with a non-linear polynomial stiffness function are used to demonstrate this methodology. The analysis is based on wavelet maps that compute time-scale information describing the localised periodicity in simulated data. Properties of these wavelet maps from transient response data are demonstrated to detect and characterise the type of non-linearities affecting the stiffness. These maps are also used to analyse transient responses from a range of airspeeds to formulate analytical functions that predict the onset of a limit cycle behaviour resulting from a Hopf bifurcation. The analysis functions developed in this paper are directly applicable only to the specific aeroelastic model but the underlying methodology used in their derivation may be considered for analysis of general non-linear systems.

ACKNOWLEDGEMENTS

The authors would like to acknowledge the generous financial support of the Structural Dynamics Branch of NASA Dryden Flight Research Center. Rick Lind was supported by a National Research Council Postdoctoral Fellowship. Kyle Snyder was supported by the NASA Academy program. Particular appreciation is extended to Tom Strganac and Jeonghwan Ko of the Texas A&M University and Andy Kurdila of the University of Florida who developed and tested the non-linear aeroelastic wind tunnel system. They provided models and simulations along with valuable insight about the dynamical characteristics of the system that was essential to correctly interpret the wavelet transform information.

REFERENCES

1. M. W. KEHOE 1995 *Proceedings of the* 80*th AGARD Structures and Materials Panel, Rotterdam, The Netherlands, AGARD-CP*-566, 1:1–1:15. Neuilly sur Seine, France: AGARD, a historical overview of flight flutter testing.
2. E. DOWELL and M. ILGAMOV 1988 *Studies in Nonlinear Aeroelasticity*. New York: Springer–Verlag.
3. S. J. WOOD and D. A. ISBELL 1986 *Proceedings of the* 30*th Annual Symposium, Beverly Hills, CA*, 202–223. Beverly Hills, CA: Society of Experimental Test Pilots. F-16/F-111 weapons flutter testing.
4. M. GIRARD and S. MCINTOSH 1996 *Proceedings of the* 40*th Annual Symposium, Beverly Hills, CA*, 190–207. Beverly Hills, CA: Society of Experimental Test Pilots. CF-18 GBU-24B/B flutter flight testing.
5. S. B. JACOBSON, R. T. BRITT, D. R. DREIM and P. D. KELLY, *Proceedings of the AIAA Structures, Structural Dynamics, and Materials Conference, Long Beach, CA*. AIAA-98-1805, Reston, VA: AIAA. Residual pitch oscillation (RPO) flight test and analysis on the B-2 bomber.
6. J. J. MEIJER and A. M. CUNNINGHAM 1995 *Proceedings of the AIAA Structures, Structural Dynamics, and Materials Conference, New Orleans, LA*. AIAA-95-1340, Reston, VA: AIAA. A semi-empirical unsteady nonlinear aerodynamic model to predict transonic LCO characteristics of fighter aircraft.
7. J. J. MEIJER and A. M. CUNNINGHAM 1992 *Proceedings of the AIAA Atmospheric Flight Mechanics Conference, Hilton Head, SC*. AIAA-92-4501, Reston, VA: AIAA. Understanding and development of a prediction method of transonic oscillation characteristics of fighter aircraft.
8. C. M. DENEGRI and M. A. CUTCHINS 1997 *Proceedings of the AIAA Structures, Structural Dynamics, and Materials Conference, Kissimmee, FL*. AIAA-97-1021, Reston, VA: AIAA. Evaluation of classical flutter analysis for the prediction of limit cycle oscillations.
9. C. M. DENEGRI and M. R. JOHNSON 1999 *Proceedings of the International Forum on Aeroelasticity and Structural Dynamics, Williamsburg, VA*. NASA-CP-1999-209136, Langley, VA: NASA. Limit cycle oscillation prediction using artificial neural networks.

10. R. LIND and M. BRENNER 1997 *Journal of Guidance, Control, and Dynamics* **20**, 597–604. Robust flutter margins of an F/A-18 aircraft from aeroelastic flight data.
11. G. STRANG and T. NGUYEN 1996 *Wavelets and Filter Banks*. Wellesley, MA: Wellesley-Cambridge Press.
12. R. LIND, M. BRENNER and S. HALEY 1997 *Proceedings of the AIAA Guidance, Navigation and Control Conference, New Orleans, LA*. AIAA-97-3836, Reston, VA: AIAA. Estimation of modal parameters using a wavelet based approach.
13. R. LIND, K. SNYDER and M. BRENNER 1997 *Proceedings of the AIAA Structures, Structural Dynamics, and Materials Conference, Long Beach, CA*. AIAA-97-1808, Reston, VA: AIAA. Investigating transient and limit cycle behaviors of a nonlinear structure by wavelet transforms.
14. S. BRAUN and M. FELDMAN 1997 *Mechanical Systems and Signal Processing* **11**, 611–620. Time–frequency characteristics of nonlinear systems.
15. T. O'NEIL and T. STRGANAC 1996 *Proceedings of the AIAA Structures, Structural Dynamics, and Materials Conference, Salt Lake City, UH*. AIAA-96-1390, Reston, VA: AIAA. Investigations of aeroelastic response for a system with continuous structural nonlinearities.
16. B. HUBBARD 1996 *The World According to Wavelets*. Wellesley MA: A.K. Peters.
17. M. MISITI, Y. MISITI, G. OPPENHIEM and J. POGGI, *Wavelet Toolbox*. Natick MA: The Mathworks.
18. Ph. TCHAMITCHIAN and B. TORRESANI 1992 In *Wavelets and their Applications*. Boston MA: Jones and Barlett Publishers. M. B. Ruskai et al. (ed.). Ridge and skeleton extraction from the wavelet transform.
19. W. J. STASZEWSKI 1998 *Journal of Sound and Vibration* **214**, 639–658. Identification of non-linear systems using multi-scale ridges and skeletons of the wavelet transform.
20. W. J. STASZEWSKI and J. E. CHANCE 1997 *Proceedings of the International Modal Analysis Conference, Orlando, FL* 1012-1016. Identification of nonlinear systems using wavelets—experimental study.
21. E. DOWELL 1990 *Proceedings of the AIAA Structures, Structural Dynamics, and Materials Conference, Long Beach, CA*. AIAA-90-1031, Reston, VA: AIAA. Nonlinear aeroelasticity.
22. J. KO, A. KURDILA and T. STRGANAC 1997 *Proceedings of the AIAA Aerospace Sciences Meeting, Reno, NV*. AIAA-97-0580, Reston, VA: AIAA. Nonlinear control theory for a class of structural nonlinearities in a prototypical wing section.
23. S. WIGGINS 1990 *Introduction to Applied Nonlinear Dynamical Systems and Chaos*. New York: Springer-Verlag.
24. J. M. T. THOMPSON and H. B. STEWART 1986 *Nonlinear Dynamics and Chaos*. Chichester, England: John Wiley and Sons.
25. J. M. T. THOMPSON and L. N. VIRGIN 1986 *International Journal of Nonlinear Mechanics* **21**, 205–216. Predicting a jump to resonance using transient maps and beats.